Supporting information

Phototunable Hopping of Microparticles Enables Surface-Selective Continuous Separation via Microfluidics

Fabian Rohne,[1] Daniela Vasquez Muñoz,[1] Yulia Gordievskaya,[1] Cevin Braksch,[1] Isabel Meier,[1] Anjali Sharma,[1] Sarah Loebner,[1] Anne Nitschke,[2] Nino Lomadze,[1] Andreas Taubert,[2] Svetlana Santer,[1] Marek Bekir,[1*]

[1] *Institute of Physics and Astronomy, University of Potsdam, 14476 Potsdam, Germany*

[2] *Institute of Chemistry, University of Potsdam, 14476 Potsdam, Germany*

S1. Details for velocity as proxy to measure hovering height

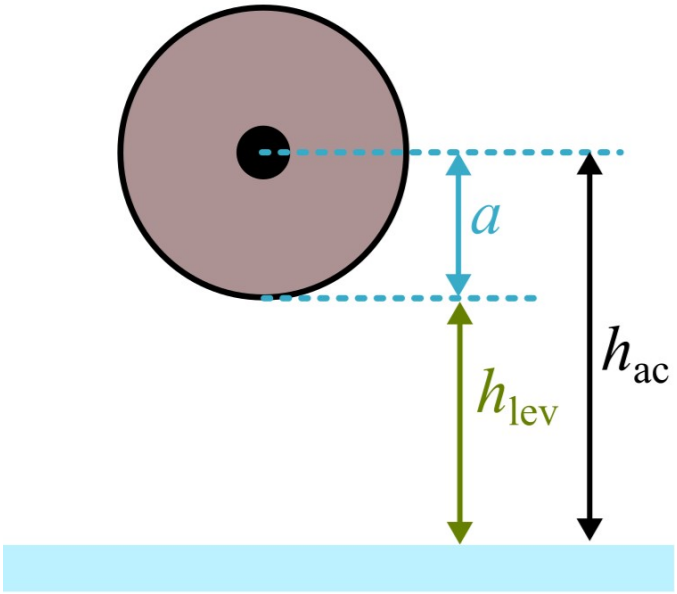

Figure S1. Schematic representation of particle levitation. The value of hac is a sum of the particle radius and the minimum distance from the bottom interface of the particle and bottom substrate.

S2. Experimental Section – additional data

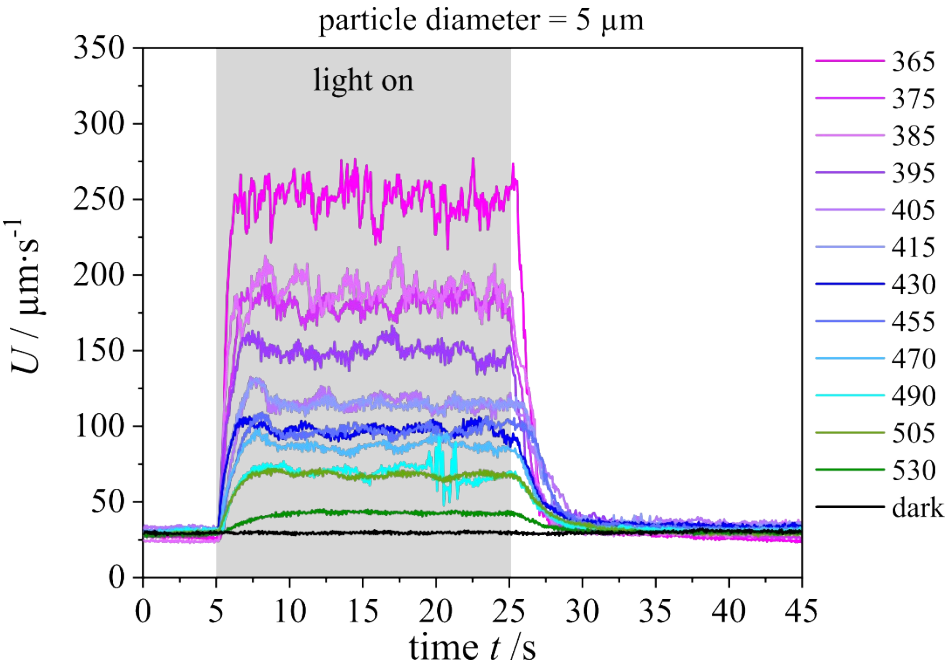

Figure S2. Time resolved velocity classified by different applied wavelengths of illumination. The grey rectangle illustrates the time of illumination. Data obtained from measurements under local light illumination. The power is set to 11.5 mW measured in front of the spatial light modulator chip.

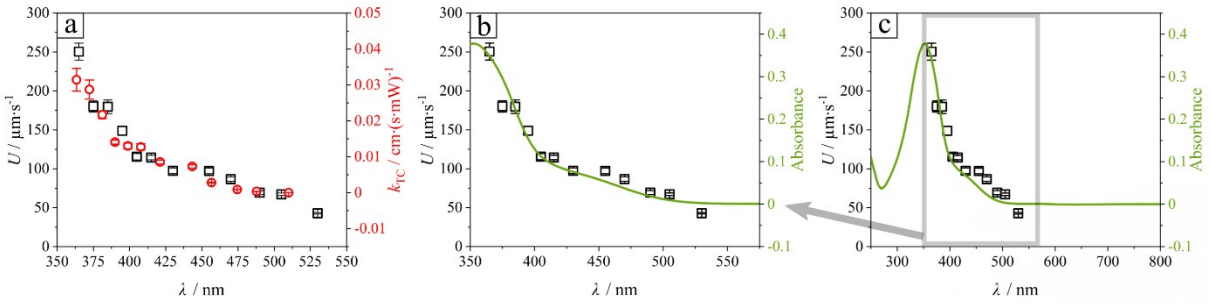

Figure S3. (a) display between velocity and trans-cis rate constant correlation. (b,c) display between velocity and the correlation of the absorbance spectrum of trans isomer.

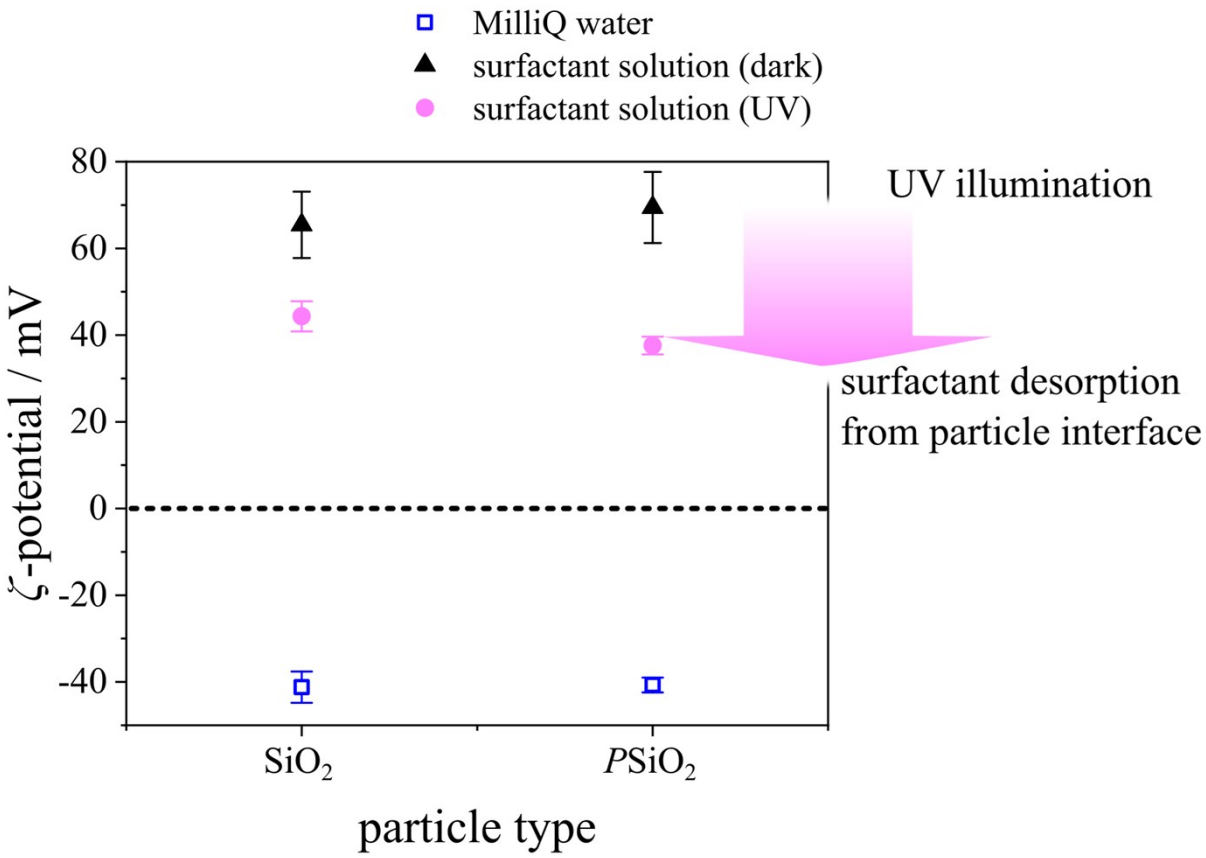

Figure S4. (a) zeta potential measurements as function of particle type, porous and non-porous particle with 5 μm diameter disperse in water and photosensitive surfactant solution.

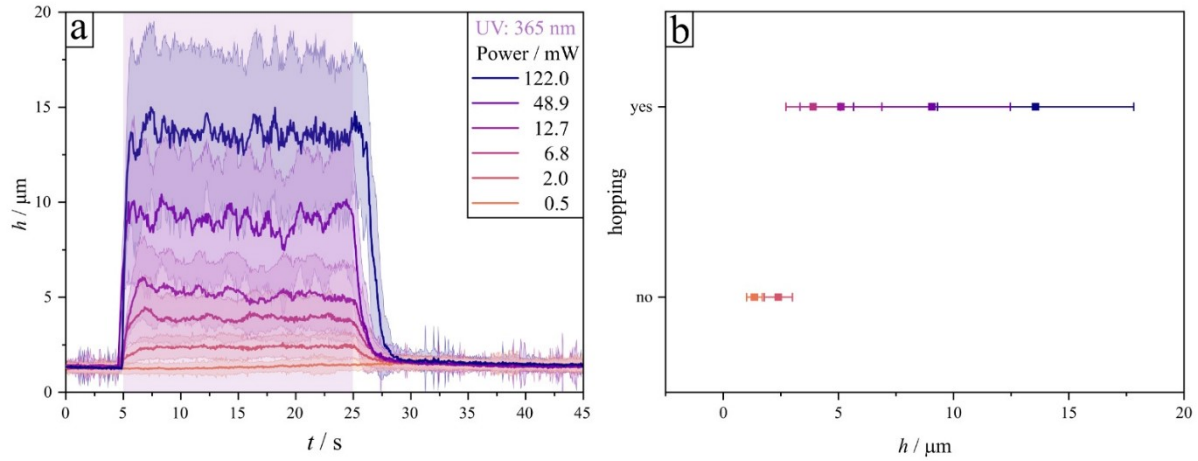

Figure S5. (a) Calculated hovering height as a function of the time. Calculation is done for a planar substrate in absence of any obstacle. (b) Observed hopping of porous particles as yes/no status classified by theoretical hovering height from applied intensity vairiation of data presented in panel (a). The Hopping was observed by precisely changing the illumination intensity of the UV light.

S3. Kinetic data for values of k_{TC}

The original experimental data and methodologies are documented in the reference.[1] A summary of relevant kinetic parameters and rate-determining values is provided in **Table S1**.

Table S1. Wavelength λ, normalized equilibrium *trans* isomer ratio c_{eq}/c_0, absolute concentration of *trans* isomers in equilibrium c_{eq}, decay time τ, rate isomerization constants of *trans-cis* isomerization k_{TC}, and *cis-trans* isomerization k_{CT} and corresponding error values abbreviated with index err

λ	c_{eq}/c_0	c_{eq}	τ	k_{TC}	$k_{TC,err}$
nm		mM	min	cm²/mW·s	cm²/mW·s
365	0.063	6.33E-02	0.50	3.14E-02	3.16E-03
375	0.068	6.77E-02	0.54	2.87E-02	2.66E-03
385	0.104	1.04E-01	0.84	2.17E-02	1.05E-03
395	0.203	2.03E-01	0.84	1.41E-02	5.50E-04
405	0.379	3.79E-01	0.79	1.30E-02	8.19E-04
415	0.414	4.14E-01	0.77	1.28E-02	8.32E-04
430	0.587	5.87E-01	0.81	8.56E-03	5.31E-04
455	0.630	6.50E-01	0.80	7.33E-03	4.61E-04
470	0.749	7.49E-01	1.48	2.83E-03	9.55E-05
490	0.844	8.44E-01	2.92	8.92E-04	1.53E-05
505	0.861	8.95E-01	4.80	3.64E-04	3.80E-06
530	0.900	9.00E-01	15.85	1.09E-04	1.61E-08

*Values were calculated from intensity, I = 1 mW/cm² and c_0 = 0.1 mM.

S4. COMSOL simulations

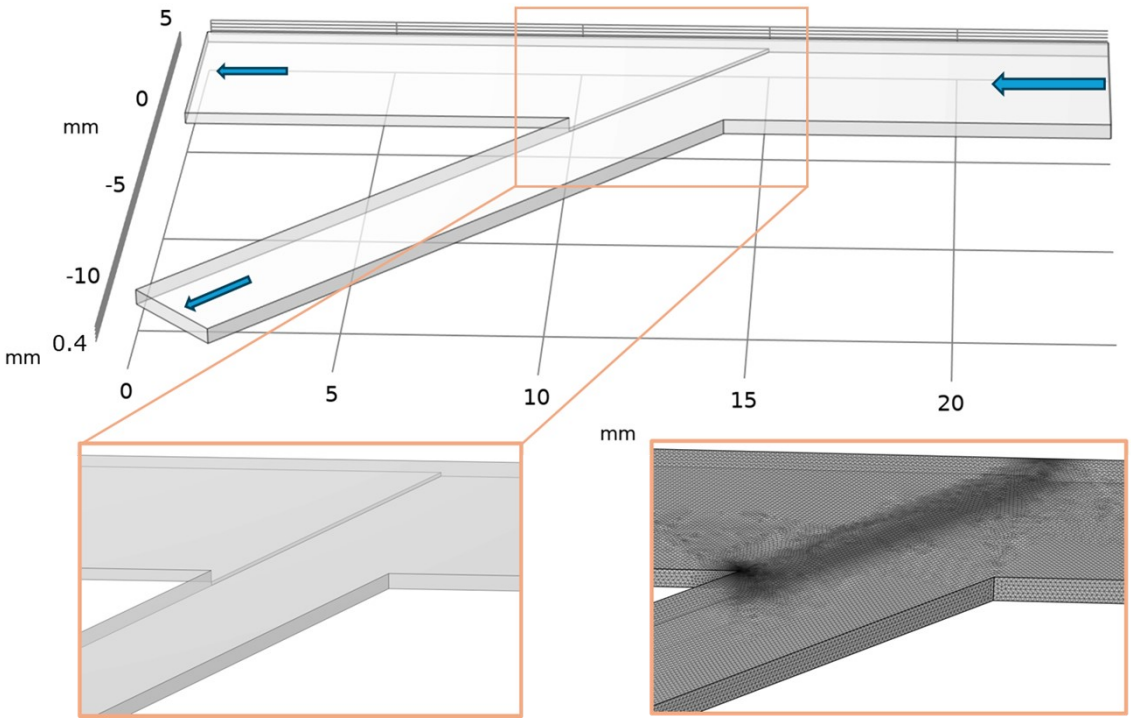

Figure S6. 3D geometry and mesh implemented in COMSOL.

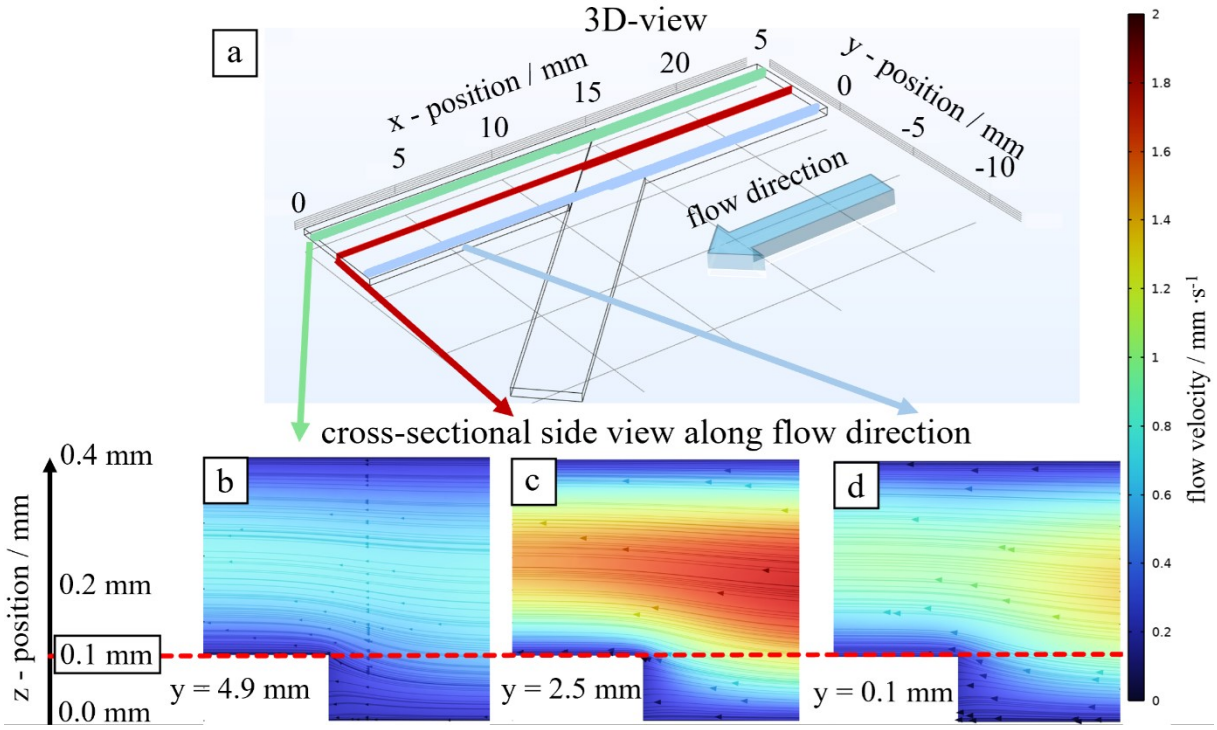

Figure S7. 3-dimensional simulation geometry (COMSOL Multiphysics) depicting the laminar flow field within the separation channel. longitudinal plane (x–z). (a) 3d view of channel geometry and illustrate longitudinal cross-sectional view in flow direction. (b,c,d) cross section at different y-positions. (b) 0.1 mm, (c) mid-with of the channel, (d) 4.8 mm. Grey arrow illustrates the flow streamline. Color mapping represents local flow velocities in mm/s.

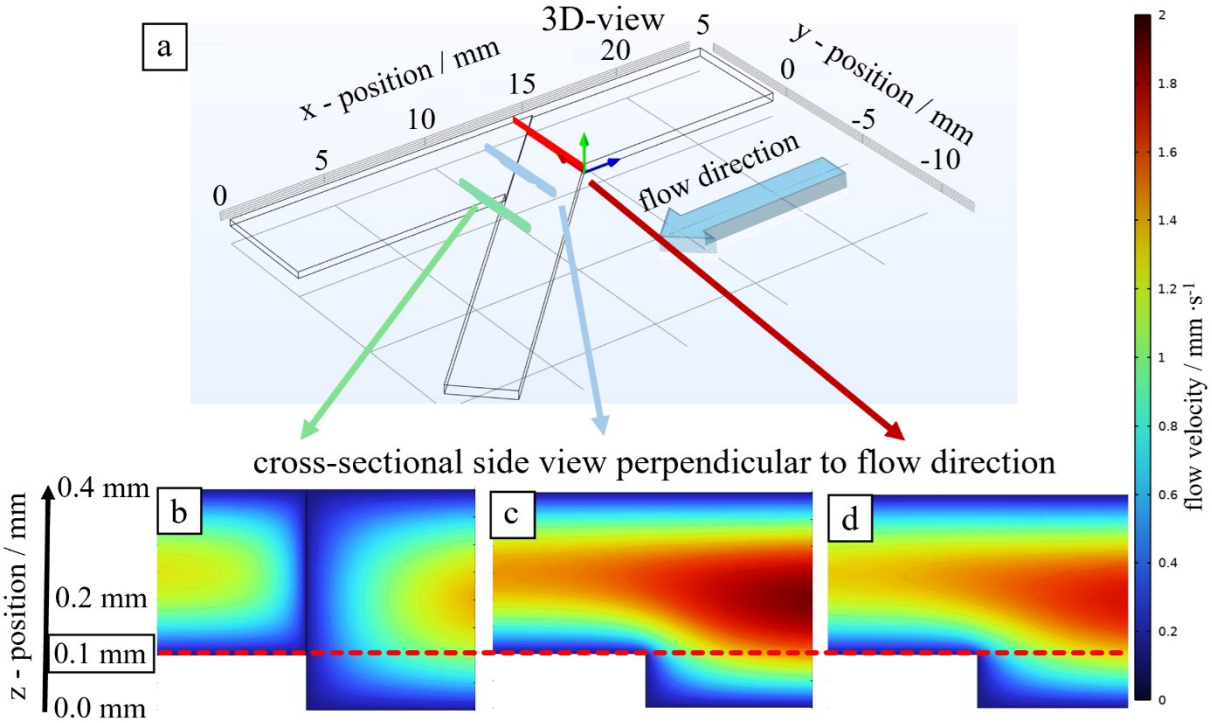

Figure S8. 3-dimensional simulation geometry (COMSOL Multiphysics) depicting the laminar flow field within the separation channel. Transverse plane (y–z). (a) 3d view of channel geometry and illustrate longitudinal cross-sectional view in flow direction. (b,c,d) cross section at different x-positions. (b) $y = 10$ mm, (c) $y = 12$ mm, (d) $y = 14$ mm. Grey arrow illustrates the flow streamline. Color mapping represents local flow velocities in mm/s.

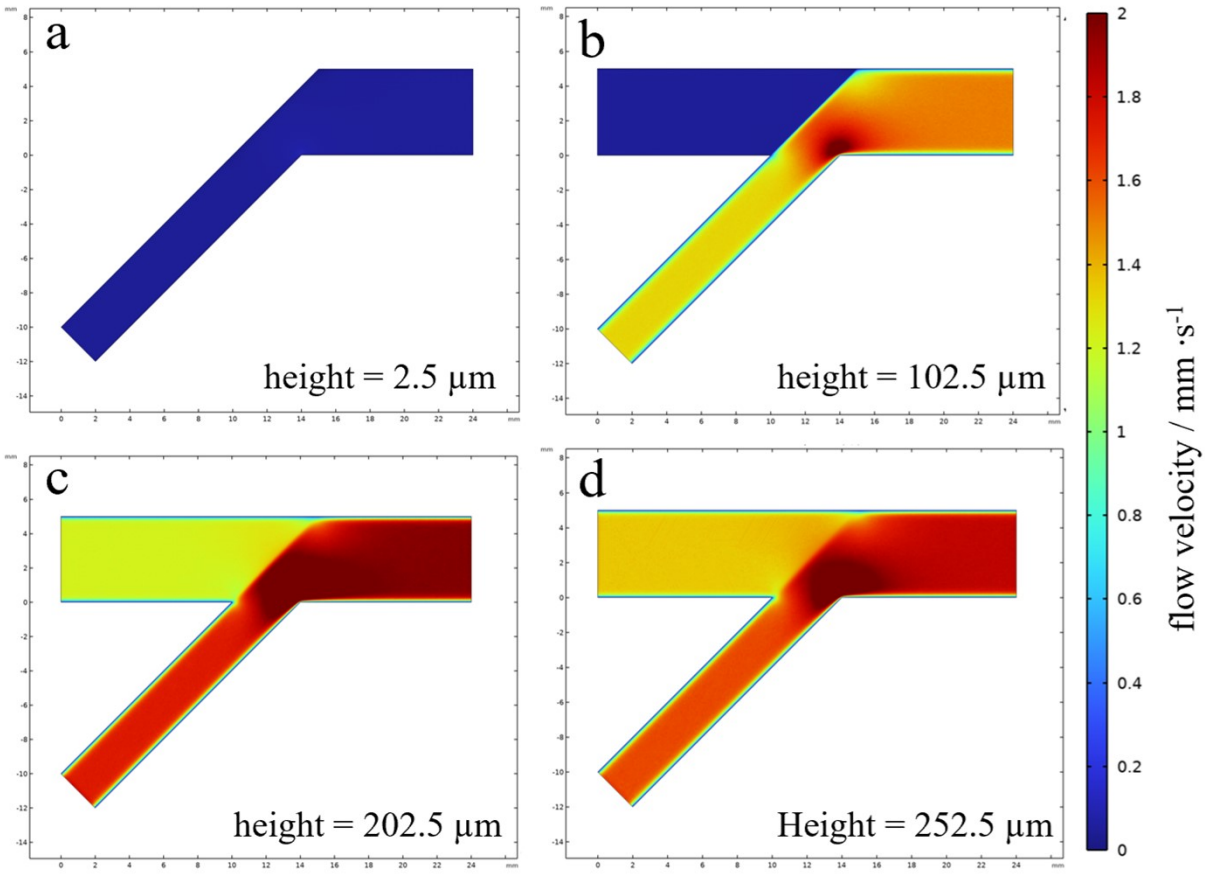

Figure S9. Simulated flow velocity distributions (top-view, x–y plane) at four different vertical positions within the channel: (a) at 2.5 µm (corresponding to particle radius); (b) at 102.5 µm (channel height plus particle radius); (c) at 202.5 µm (well above the channel height, (d) at 252.5 µm (center channel height). These simulations highlight the spatial variation in flow velocity experienced by particles depending on their vertical position, essential for guiding separation behavior. Color mapping represents local flow velocities in mm/s.

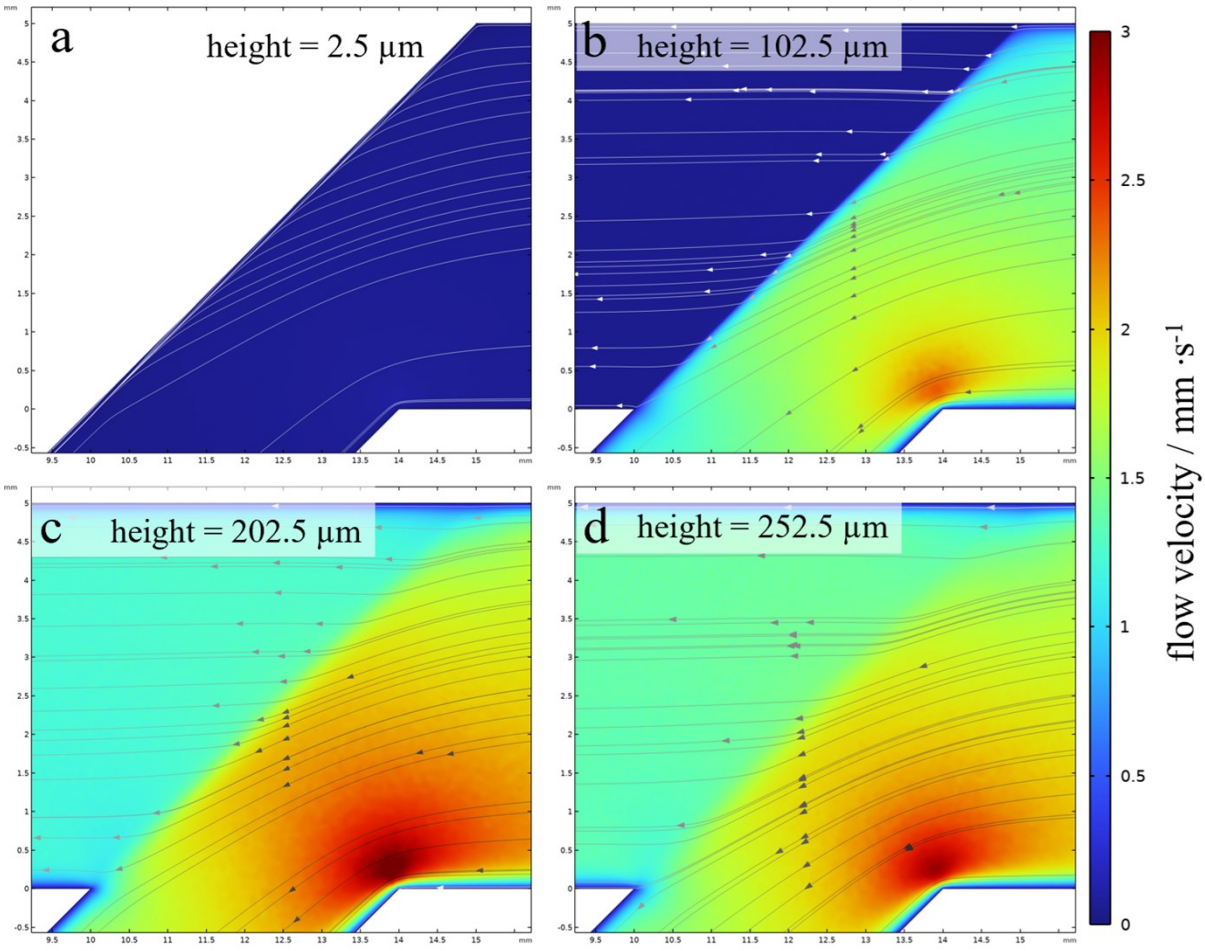

Figure S10. Simulated flow velocity distributions (top-view, x–y plane) at four different vertical positions within the channel: (a) at 2.5 µm (corresponding to particle radius); (b) at 102.5 µm (channel height plus particle radius); (c) at 202.5 µm (well above the channel height)(d) at 252.5 µm (center channel height). These simulations highlight the spatial variation in flow velocity experienced by particles depending on their vertical position, essential for guiding separation behavior. Color mapping represents local flow velocities in mm/s. Different display style to data presented in Figure S7. Grey arrows illustrates the flow field.

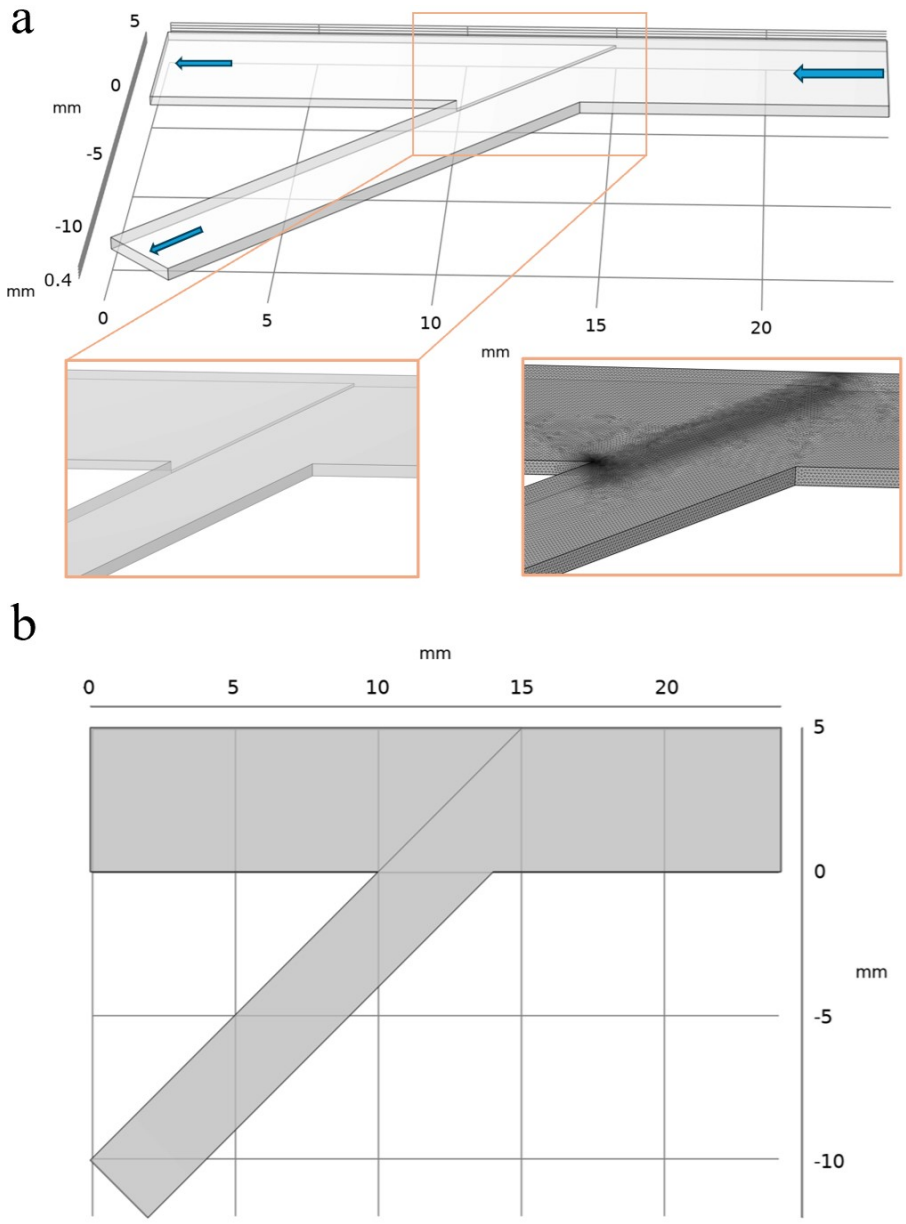

Figure S11. Details of simulation box. (a) 3d view with insets highlighting transition from bottom to upper channel and representative mesh boxes for simulation. (b) top view of the channel.

S5. Details about separation efficiency calculation

This section describes the details of the measurement condition to display the effectiveness of particle separation.

To this end, porous silica ($PSiO_2$) and non-porous (plain) silica (SiO_2) microparticles with a diameter of 5 µm were mixed in a 1:2 ratio and subsequently dispersed in an aqueous fluorescein–surfactant solution. Fluorescein forms a complex with cationic surfactants, which, above the critical micelle concentration (CMC), leads to a pronounced enhancement of the dye's fluorescence emission (Figure S10a). Due to their significantly higher surface area, porous microparticles facilitate increased adsorption of both the surfactant and the dye at the particle interface, resulting in a stronger fluorescence signal when imaged using the FITC channel (Figure S10b). The dispersion was then introduced into a microfluidic channel, and the imaging objective was positioned near the channel inlet to ensure that only a defined population of particles was present in the field of view during flow-based imaging

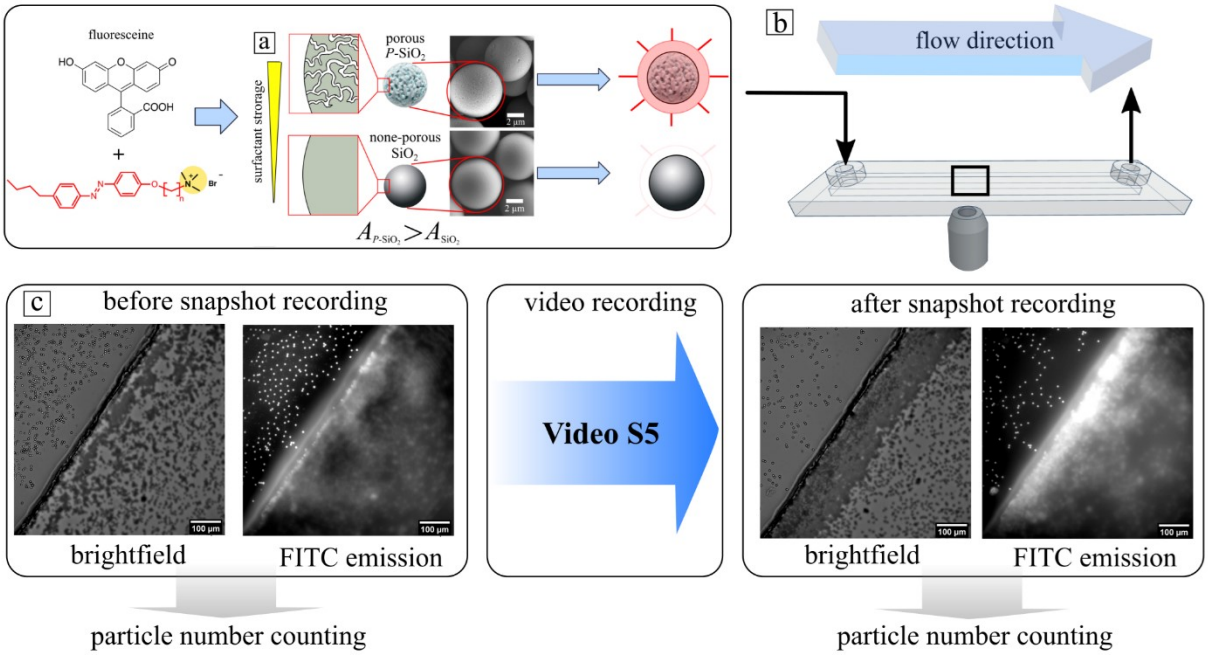

Figure S12. Overall illustration of measurement conditions to display separation effectiveness. (a) Mixing fluoresceine (c = 15 µM) with surfactant solution (c = 1 mM) with (b) porous and plain silica microparticles (D = 5 µm, $c_{particles,total}$ = 0.5 mg/mL, ratio $PSiO_2/SiO_2$ = 1/2). (c) The dispersion is injected into the microfluidic channel, where the data recording is performed at the wall position. (d) Principal illustration of measurement performance from a series of snapshots in combination with video recording. Before the video recording snapshots are taken to count the microparticles in bright field and emission signal in top and bottom focus. Then video recording was performed. After that again snapshots are recorded. The Snapshot series is displayed from **Figure S13–Figure S20**and summarized in **Figure 7 main article**.

To display the effectiveness of separation we measured a separation for 30 s in Video S5. The video includes combination of snapshots in bright field and FITC emission recording.

Snapshot recording:

Every snapshot is recorded between the video recording. From the snapshots, the number of total particles in the bright field image and that of the porous microparticles in the FITC emission image are counted. This allows us to distinguish between the ratio of porous and plain microparticles after running the video file **Video S5**. For details see Supporting Information **Section S5.1**. The series of snapshots is presented as raw images and processed data treatment in **Figure S13–Figure S20** and following image treatment for subsequent particle counting, is summarized in **Figure 7** of the **main article**.

Video recording

The experimental video shows a forward flow under light illumination with blue light (λ = 365 nm, P = 11.5 mW) for 45 s.

S5.1 Raw images of snapshots before experimental videos

Before: Top focus - brightfield

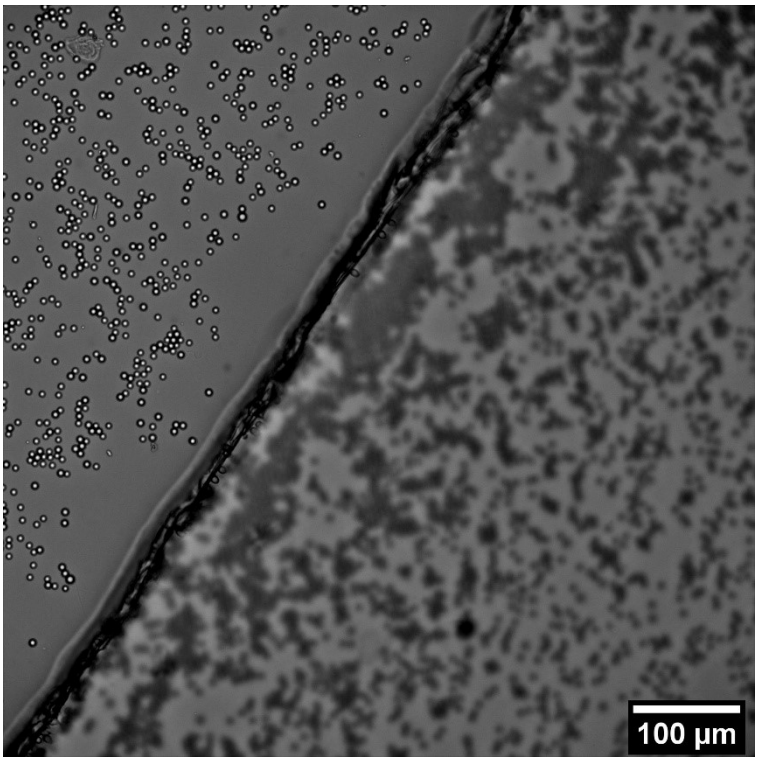

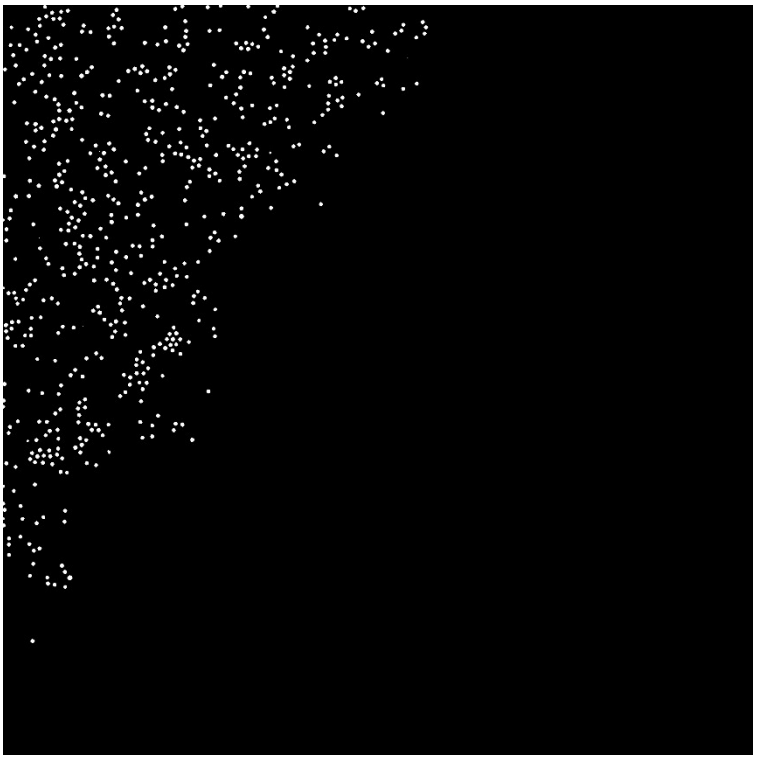

Figure S13. Bright field (top) and black and white (bottom) of local particle mixture of porous ($PSiO_2$) and plain (SiO_2) microparticle (D = 5 µm) immersed in azobenzene containing solution in complex with fluoresceine dye. Counted number of particles: 556

Before: Top focus - emission

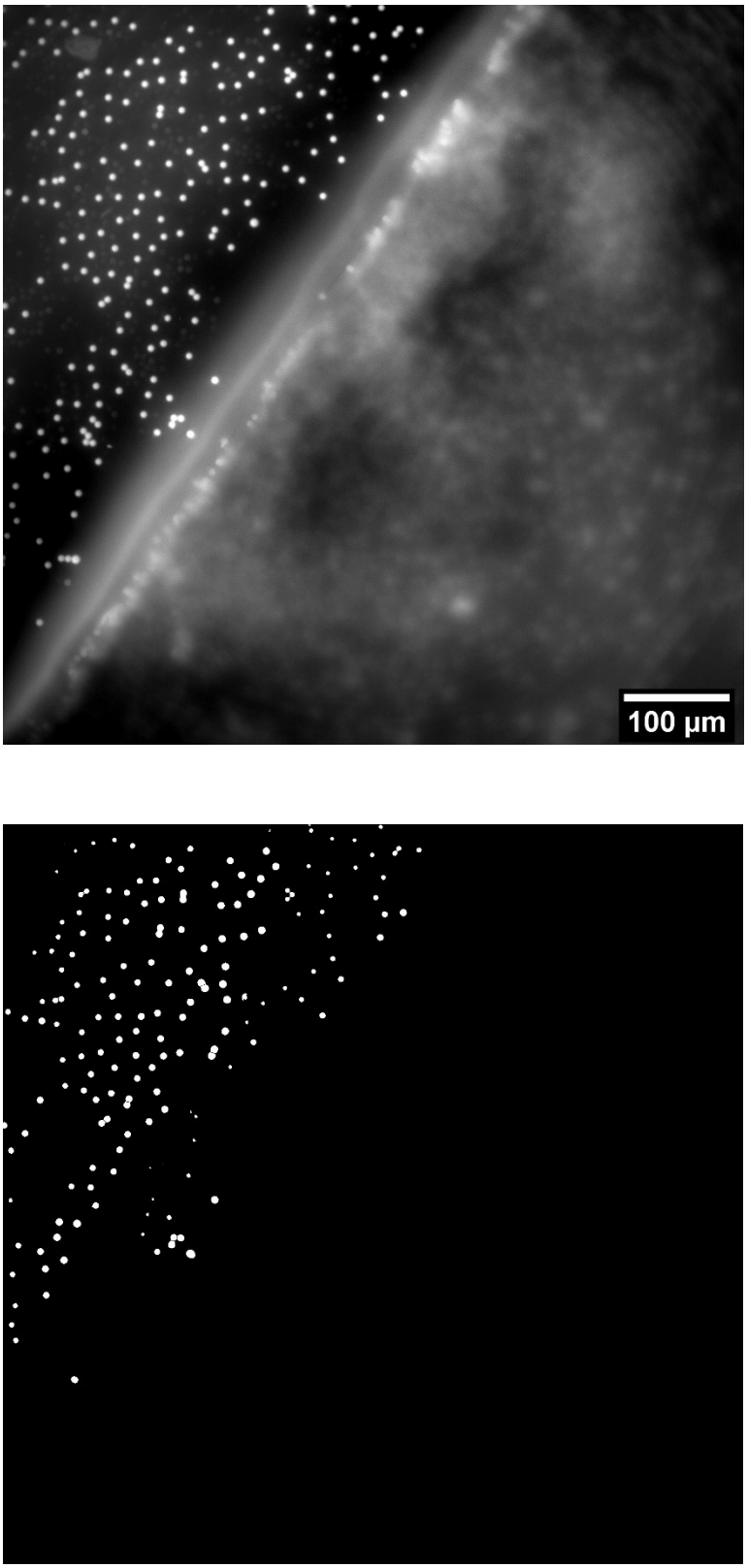

Figure S14. Emission (top) and black and white (bottom) of local particle mixture of porous ($PSiO_2$) and plain (SiO_2) microparticle (D = 5 µm) immersed in azobenzene containing solution in complex with fluoresceine dye. Counted number of particles: 209

After: Top focus - brightfield

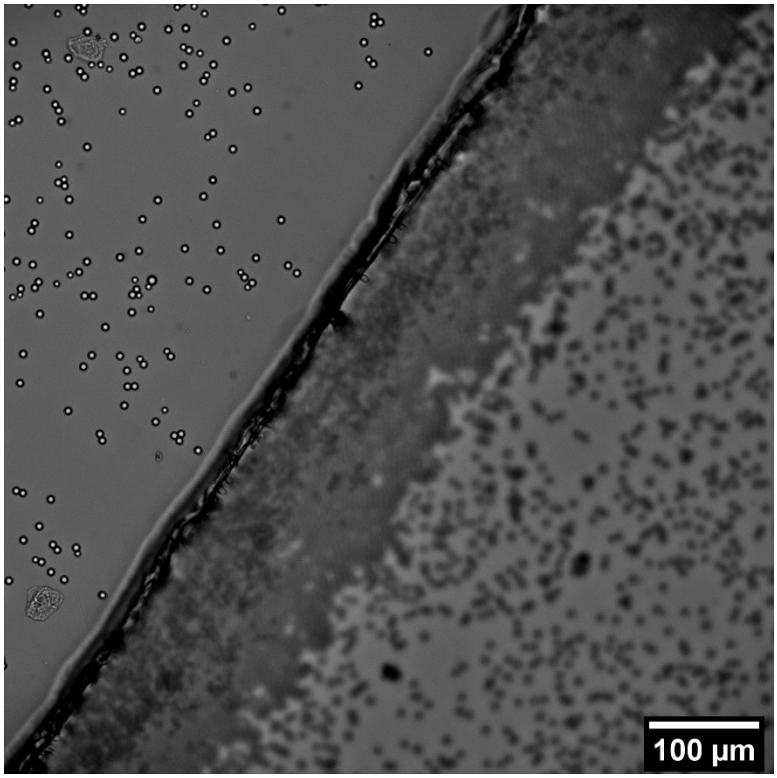

Figure S15. Bright field (top) and black and white (bottom) of local particle mixture of porous ($PSiO_2$) and plain (SiO_2) microparticle (D = 5 µm) immersed in azobenzene containing solution in complex with fluoresceine dye. Counted number of particles: 151

After: Top focus - emission

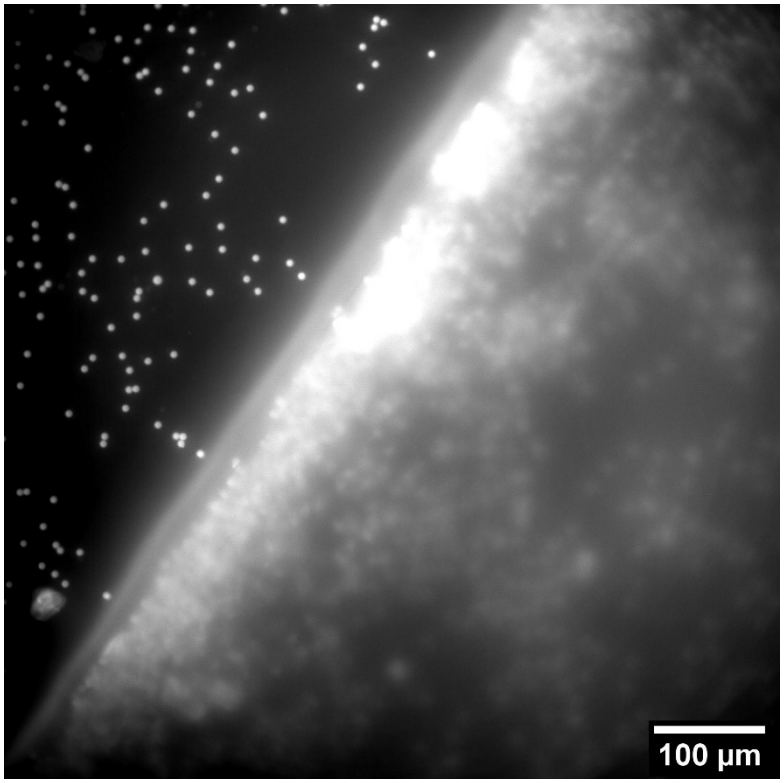

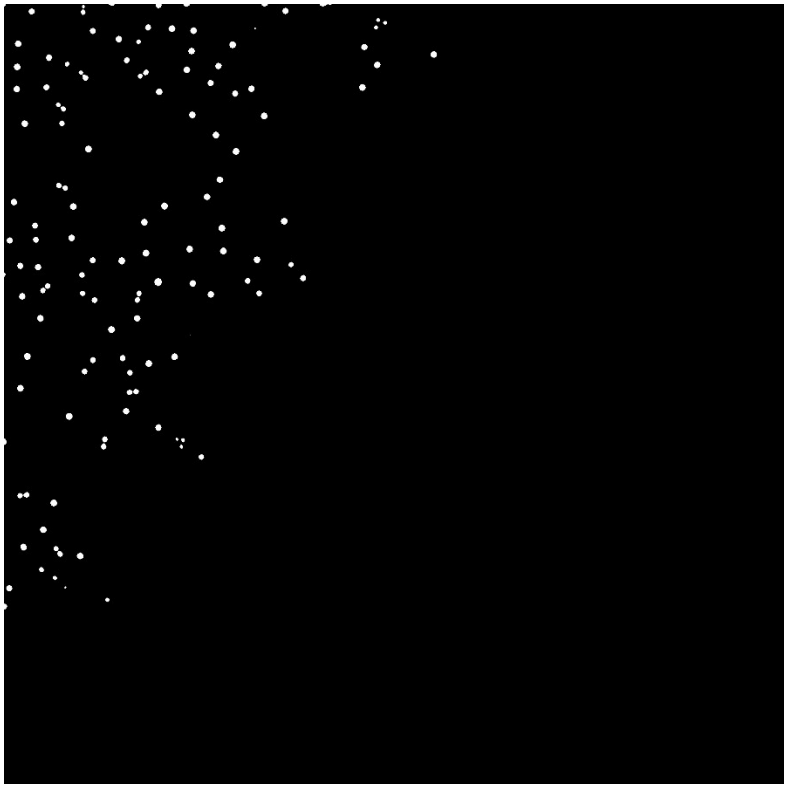

Figure S16. Emission (top) and black and white (bottom) of local particle mixture of porous ($PSiO_2$) and plain (SiO_2) microparticle (D = 5 µm) immersed in azobenzene containing solution in complex with fluoresceine dye. Counted number of particles: 129

Before: bottom focus - brightfield

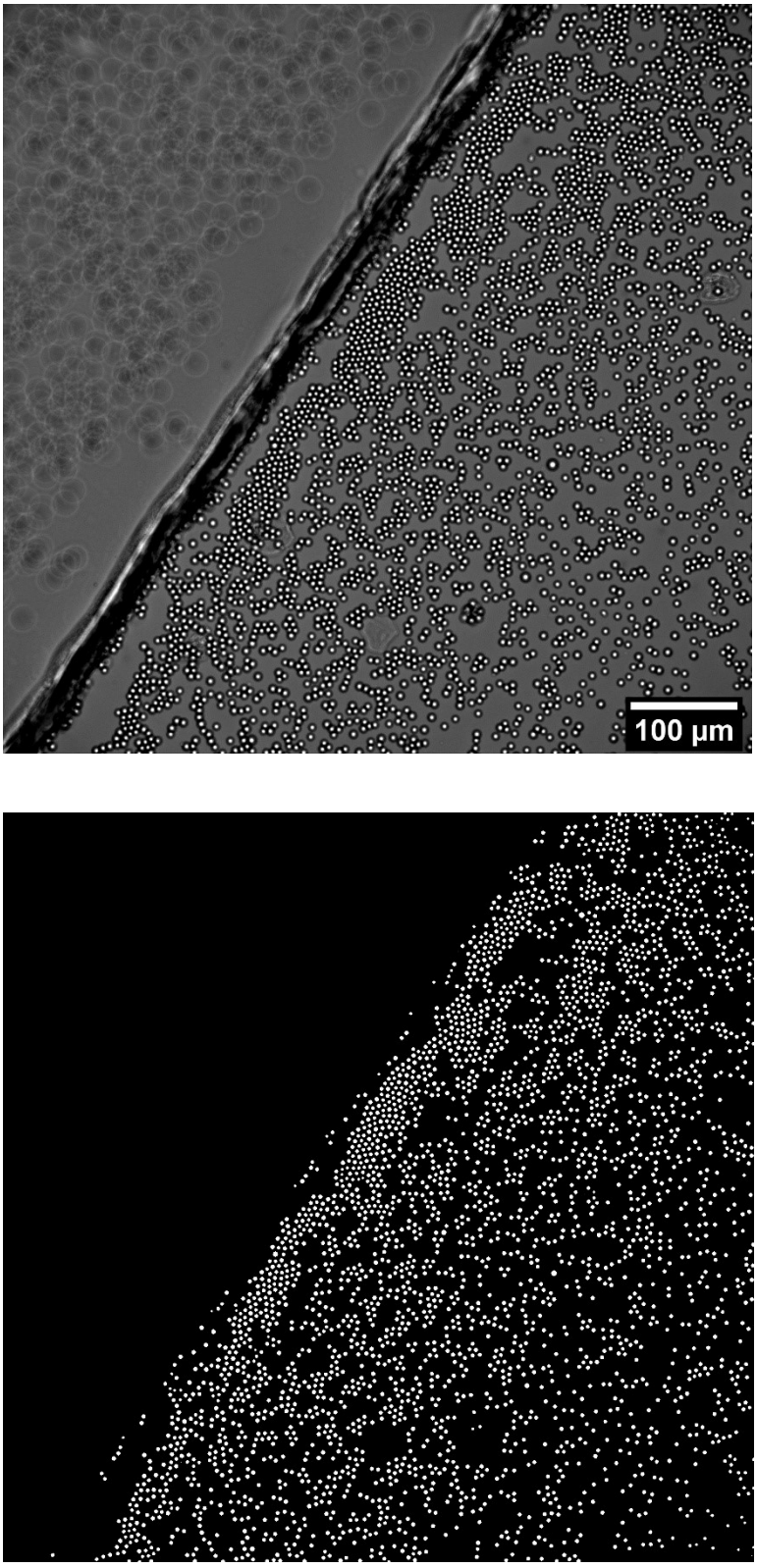

Figure S17. Bright field (top) and black and white (bottom) of local particle mixture of porous ($PSiO_2$) and plain (SiO_2) microparticle (D = 5 µm) immersed in azobenzene containing solution in complex with fluoresceine dye. Counted number of particles: 3191

Before: bottom focus - brightfield

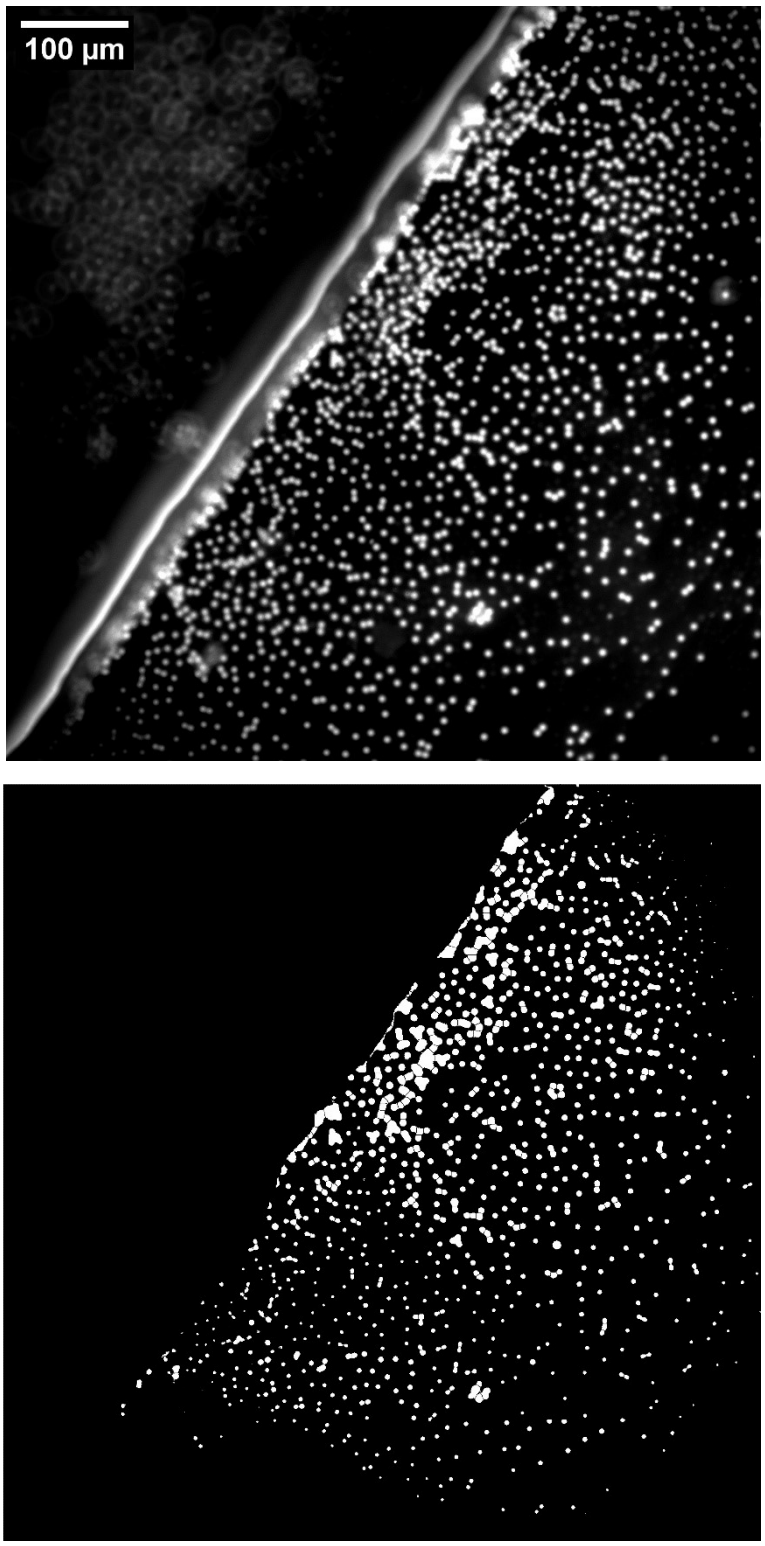

Figure S18. Emission (top) and black and white (bottom) of local particle mixture of porous ($PSiO_2$) and plain (SiO_2) microparticle (D = 5 µm) immersed in azobenzene containing solution in complex with fluoresceine dye. Counted number of particles: 1095

After: bottom focus - brightfield

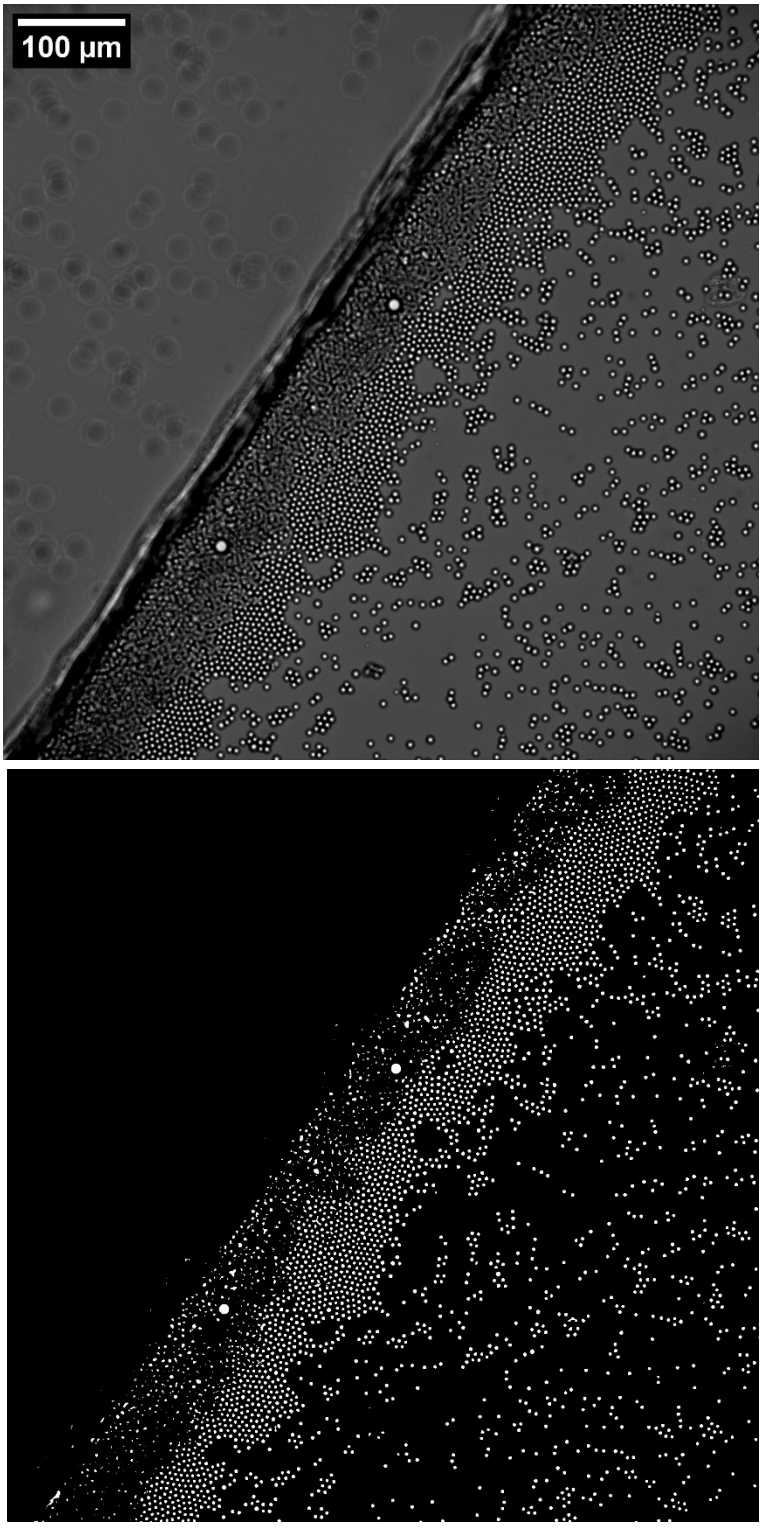

Figure S19. Bright field (top) and black and white (bottom) of local particle mixture of porous ($PSiO_2$) and plain (SiO_2) microparticle (D = 5 µm) immersed in azobenzene containing solution in complex with fluoresceine dye. Counted number of particles: 3903

After: bottom focus - brightfield

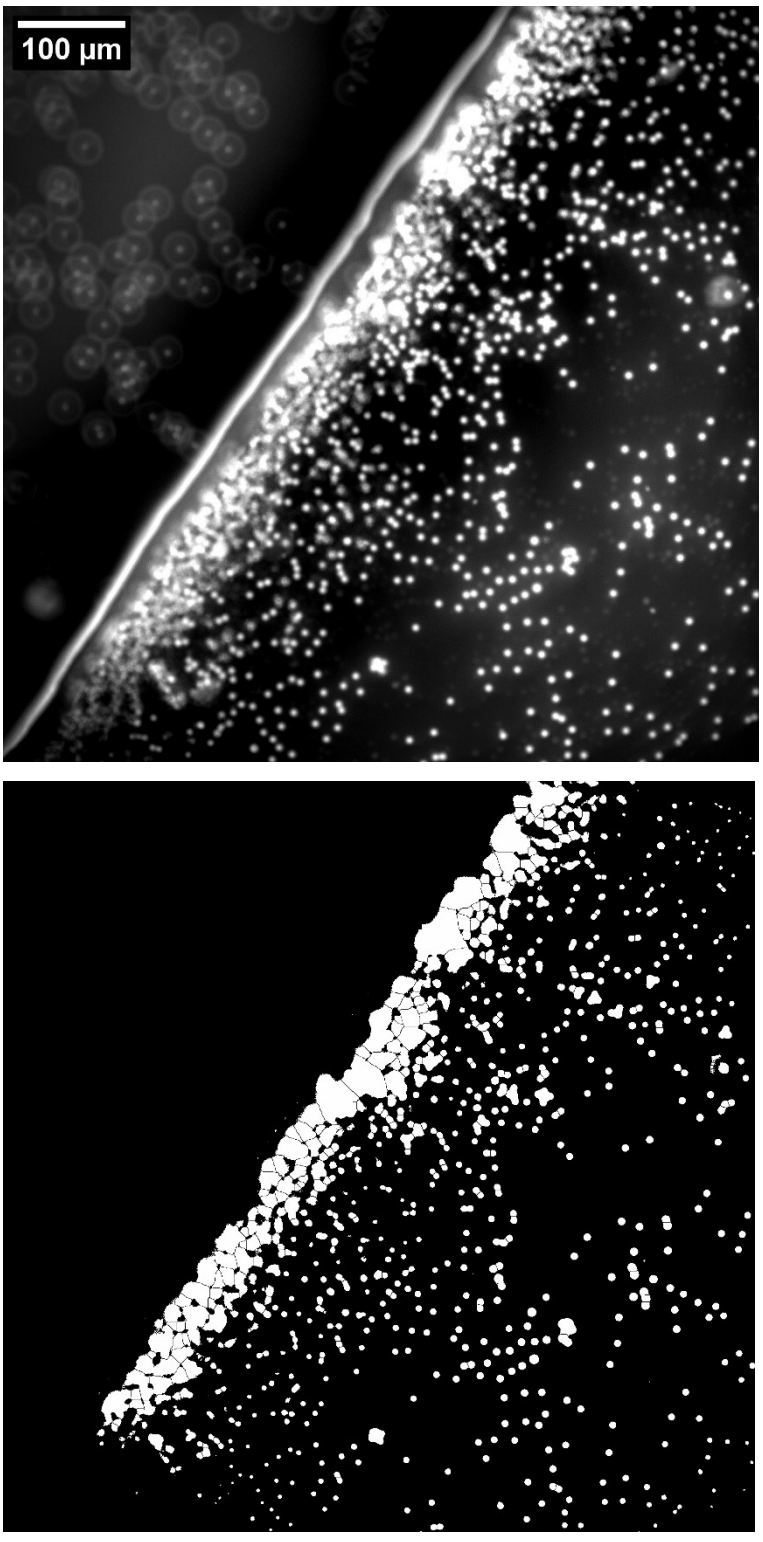

Figure S20. Emission (top) and black and white (bottom) of local particle mixture of porous ($PSiO_2$) and plain (SiO_2) microparticle (D = 5 µm) immersed in azobenzene containing solution in complex with fluoresceine dye. Counted number of particles: 902

S5.2 Experimental data treatment

To quantify the number of microparticles in both bright-field and fluorescence emission images, all image data were first converted into binary format using a thresholding procedure. Due to more favorable illumination conditions under red light (λ = 625 nm), bright-field images consistently exhibited higher contrast and were therefore more readily thresholded. Consequently, we present the image processing workflow using fluorescence emission images, which generally required more careful adjustment due to lower contrast and background noise.

Image analysis was performed using the Fiji distribution of ImageJ, without the need for additional plugin packages. All images were processed consistently following this protocol.

S1. Spatial background contrast manipulation with "Normalized Local Contrast" algorithm

a. Set Parameters: Block radius x and y: 400 pixels
b. Standard deviation: 3.00
c. Center on
d. Stretch off

S2. Image thresholding with "Yen algorithm", default set

S3. The binary pixel information is treated with Binary Options standard plugin:

a. Do: Watershed

S4. **Crop parts, which do not belong to focus. Example: If top focus parts from bottom focus are removed and vice versa**

This yields finally a clear threshold image displayed in **Figure S13–Figure S20**. Then the number of particles is calculated via:

S5. The black points (particles) are calculated with Analyse Particles standard plugin:

a. Size in pixel^2: 3–infinite → (to neglect noise)

Since the size was not necessary, we only count the number of particles.

S5.3 Particle counting

From snapshots displayed in **Figure S13–Figure S20**. the binary mixture of porous (*P*-SiO_2) and plain (SiO_2) particles (adjusted ratio of 1:2) are counted before and after **Video S5**. The porous particles are labelled fluoresceine, while plain particles are unlabeled. From the bright field image, the total number of particles N_{total} are known. The emission image only reveals the number of porous particles N_{PSiO2}. With this knowledge we calculated the number of plain particles N_{SiO2} via:

$$N_{SiO_2} = N_{total} - N_{PSiO_2}, \quad \text{S1}$$

where with the relation $N_{total} = N_{bright\ field\ image}$ and $N_{PSiO2} = N_{emission}$ equation S1 can be rewritten into:

$$N_{SiO_2} = N_{bright\ field\ image} - N_{emission}. \quad \text{S2}$$

Data in **Figure 7** shows the values of N_{total} and N_{PSiO2} before and after **Video S5**. To calculate the ratio of porous particle normalized to total number of particles $\frac{N_{PSiO_2}}{N_{SiO_2} + N_{PSiO_2}}$, we use following equation:

$$\frac{N_{PSiO_2}}{N_{total}} = \frac{N_{PSiO_2}}{N_{SiO_2} + N_{PSiO_2}} = \frac{N_{emission}}{N_{brightfield\ image}}. \quad \text{S3}$$

S5.4 Separation efficiency

Further we calculated from values in **Figure S13–Figure S20** the separation efficiency as a function of the separation cycle. To calculate the separation efficiency we used the equation from reported literature:[2]

$$separation\ efficiency\ for\ SiO_2 = 1 - \frac{N_1}{N_{feed}} = 1 - \frac{N_{emission}}{N_{brightfield\ image}}, \quad \text{S4}$$

and for

$$separation\ efficiency\ for\ PSiO_2 = \frac{N_1}{N_{feed}} = \frac{N_{emission}}{N_{brightfield\ image}}, \quad \text{S5}$$

with $N_1 = N_{\text{emission}}$ and $N_{\text{feed}} = N_{\text{brightfield image}}$ as the particle number remained and initially in the microfluidic chamber.

S6. Porosity Determination of Porous and Plain Microparticles.

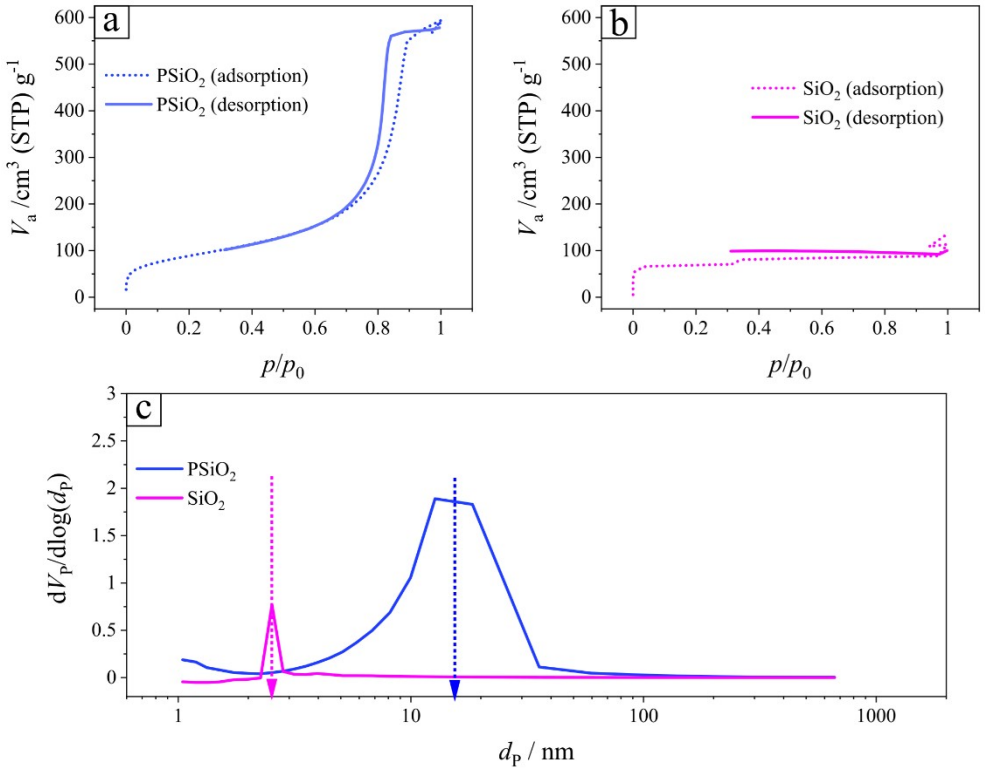

Figure S21. (a) Nitrogen adsorption and desorption isotherm of pure (a) porous ($PSiO_2$) particles and (b) non-porous (SiO_2) silica microparticles. (c) calculate pore diameter from data in panel a and b.

Data in **Figure S21** display the adsorbed saturation volume $V_{a,sat}$ for the pure porous particle sample (**Figure S21**a) and reveals a multiporous structure due to a dual-stage saturation with a maximum adsorption of 565 $cm^3 \cdot g^{-1}$ at the normalized pressure range $\Delta p/p_0$ = 0.8–1.0. This indicates the presence of macropores with a calculated average pore diameter of 12 nm (**Figure S21**c). In contrast, the non-porous particle sample exhibits a monophasic saturation curve, indicating a smoother surface without larger pore structures with a pore diameter of 2.5 nm (**Figure S21**c), however with a measurable $V_{a,sat}$ value of approximately 114 $cm^3 \cdot g^{-1}$. This is attributed to the intrinsic mesoporosity of silica where even non-porous silica particles can permit limited nitrogen adsorption.

The ratio of $V_{a,sat,PSiO2}$ and $V_{a,sat,SiO2}$, 565 $cm^3 \cdot g^{-1}$/114 $cm^3 \cdot g^{-1}$ = 4.95 indicates approximately a fifth-fold bigger pore volume.

S7. Calculation of the Sedimentation Time

The sedimentation time for the system was calculated using the Stokes Equation.

$$v_s = \frac{d^2 g(\rho_p - \rho_f)}{18\eta}, \quad \text{S6}$$

$\eta = 1.0014 \cdot 10^{-3}\, Pa \cdot s$ from reference [3]

$d = 3 \cdot 10^{-6}\, m$ Main article

$\rho_f = 1040\ kg\ m^{-3}$ from reference [4]

$\rho_p = 1800\ kg\ m^{-3}$ Main article

$g = 9.81\ m\ s^{-1}$ from reference [5]

The maximum sedimentation time is calculated as the channel height divided by the sedimentation velocity.

$$t_{max} = \frac{h}{v_s} = 107.5\ s. \quad \text{S7}$$

$h = 0.4 \cdot 10^{-3}\, m$ Main article

Accordingly, all particles are sedimented after 107.5 seconds. We calculated the value using the smallest particles in the publication and the lowest density, since this yields the lowest sedimentation velocity. All other particles will sediment faster.

In a continuous process in which particles are injected into an external laminar flow, the particles are carried with the flow during sedimentation. This means we can calculate the distance *x* a particle travels with the flow until it is fully sedimented. We propose that the velocity of the particle is given as a superposition of the velocity in flow direction

$$u = \frac{U_0 z}{2\ h}\left(1 - \frac{z}{h}\right), \quad \text{S8}$$

and the sedimentation velocity perpendicular to the flow direction

$$v\ =\ v_s = \frac{d^2 g(\rho_p - \rho_f)}{18\eta}, \quad \text{S9}$$

Since the sedimentation velocity is constant in time and independent of u, the motion is uniform. Accordingly, the z coordinate is given by

$$z(t)\ =\ v_s \cdot t, \quad \text{S10}$$

From Equation S11 we can calculate the sedimentation time of a particle from the top to the bottom:

$$t_{sed} = \frac{h}{v_{s,}} \qquad \text{S11}$$

To calculate the distance *x,* we insert Equation S11 into Equation S9 and integrate over the sedimentation time

$$u = \frac{U_0 v_s \cdot t}{2\ h}\left(1 - \frac{v_s \cdot t}{h}\right), \qquad \text{S12}$$

$$x = \int_0^{t_{sed}} \frac{U_0 v_s \cdot t}{2\ h}\left(1 - \frac{v_s \cdot t}{h}\right) dt\,, \qquad \text{S13}$$

$$= \frac{U_0}{2}\left(\int_0^{t_{sed}} \frac{v_s \cdot t}{h}\, dt - \int_0^{t_{sed}} \left(\frac{v_s \cdot t}{h}\right)^2 dt\right), \qquad \text{S14}$$

$$= \frac{U_0}{2}\left(\left[\frac{v_s \cdot t^2}{2h}\right]_0^{t_{sed}} - \left[\frac{v_s^2 \cdot t^3}{3h^2}\right]_0^{t_{sed}}\right), \qquad \text{S15}$$

$$= \frac{U_0}{2}\left(\left[\frac{v_s \cdot h^2}{2h \cdot v_s^2} - 0\right] - \left[\frac{v_s^2 \cdot h^3}{3h^2 \cdot v_s^3} - 0\right]\right), \qquad \text{S16}$$

$$= \frac{U_0}{2}\left(\frac{h}{2v_s} - \frac{h}{3v_s}\right), \qquad \text{S17}$$

$$= \frac{U_0}{12} \cdot \frac{h}{v_s}, \qquad \text{S18}$$

$$= \frac{U_0}{12} \cdot \frac{h \cdot 18\eta}{d^2 g(\rho_p - \rho_f)} \qquad \text{S19}$$

$$\approx 44\ mm \qquad \text{S20}$$

$\eta = 1.0014 \cdot 10^{-3}\ Pa \cdot s$	from reference [3]
$d = 3 \cdot 10^{-6}\ m$	Main article
$\rho_f = 1040\ kg\ m^{-3}$	from reference [4]
$\rho_p = 1800\ kg\ m^{-3}$	Main article
$h = 0.54\ mm$	Main article
$U_0 = 16\ mm\ s^{-1}$	from reference [6]
$g = 9.81\ m\ s^{-1}$	from reference [5]

S8. Stokes Number

The Stokes number is the ratio of the characteristic time of a particle τ_v to a characteristic time of the flow. Thus, it is a dimensionless constant giving us a measure for the response of the particle to the external flow expressing, the 'particle inertia':

$$St = \frac{\tau_\mathrm{v}}{\tau_\mathrm{f}}. \qquad \text{S21}$$

The characteristic time of the particle τ_v depends on the particle diameter D and density ρ_p

$$\tau_\mathrm{v} = \frac{\rho_\mathrm{p} D^2}{18\mu_\mathrm{f}}, \qquad \text{S22}$$

where μ_f is the fluid viscosity. Since all experiments were performed with the same particles and in the same solution, we can give one constant value for τ_v:

$$\tau_\mathrm{v} = \frac{1.8\ \mathrm{g \cdot cm^{-3}} \cdot (5 \pm 1.5\ \mu m)^2}{18 \cdot 1.0016\ \mathrm{mPa \cdot s}} \approx (45 \pm 27)\ \mu\mathrm{s}, \qquad \text{S23}$$

with μ_f as the viscosity of water at room temperature. We assume that the small concentration of azobenzene surfactant does not change the viscosity significantly. The large error of the constant is a result of the heterogeneity of the particle diameter $(5 \pm 1.5\ \mu\mathrm{m})$ of the sample used. However, the characteristic time of the particle is far below our time resolution of 0.03 s, meaning that the characteristic response to changes in the external flow is below our time resolution. Especially for the process of lifting, a particle immediately follows the flow at the corresponding height, and thus the particle velocity is determined by the flow velocity during lifting and not by its own inertia.

To calculate the Stokes number, we must determine the characteristic time of the flow as well. We do this for a single sedimented particle. The particle is only affected by the flow at its position, and thus the timescale for the flow is the ratio of the particle size to flow velocity:

$$\tau_\mathrm{f} = \frac{d}{u_\mathrm{f}}. \qquad \text{S24}$$

Inserting S21 and S23 into S20 gives us:

$$St = \frac{\rho_\mathrm{p} \cdot d \cdot u_\mathrm{f}}{18\mu_\mathrm{f}}, \qquad \text{S25}$$

with the flow velocity $37\ \mu\mathrm{m} \cdot \mathrm{s}^{-1}$ at the center of a sedimented particle of diameter $5\ \mu\mathrm{m}$ reported by Bekir et al.[7] we get:

$$St = \frac{1.8\mathrm{g} \cdot \mathrm{cm}^{-3} \cdot 5\ \mu\mathrm{m} \cdot 37\ \mu\mathrm{m} \cdot \mathrm{s}^{-1}}{18 \cdot 1.0016\ \mathrm{Pa} \cdot \mathrm{s}} \approx 0.000332 \pm 0.000100 \qquad \text{S26}$$

The Stokes number is much smaller than 1, meaning that the particle follows the flow. Thus, the particle velocity is determined by the fluid velocity when particle-particle interactions are negligible.

S9. Calculation of Crossing Time

Sample continuous operation

For continuous operation, the feed suspension was prepared with an adjusted number ratio of porous to plain microparticles (d = 5 µm) of 1:2. The total particle mass concentration of the sample was set to c_{total} = 0.3 mg/mL. Considering the mixing ratio, the mass fraction of porous particles corresponds to approximately 0.33 of the total particle concentration. Consequently, the absolute concentration of porous particles in the feed suspension is given by

$$c_{porous} = 0.33 \cdot c_{\text{total}} = 0.33 \cdot 0.3\frac{mg}{mL} = 0.1\frac{mg}{mL} \quad \text{S27}$$

Thus, the suspension contains 0.10 mg mL^{-1} porous colloidal microparticles, while the remaining 0.20 mg mL^{-1} corresponds to plain particles, maintaining the prescribed 1:2 porous-to-plain particle ratio in the continuous separation feed.

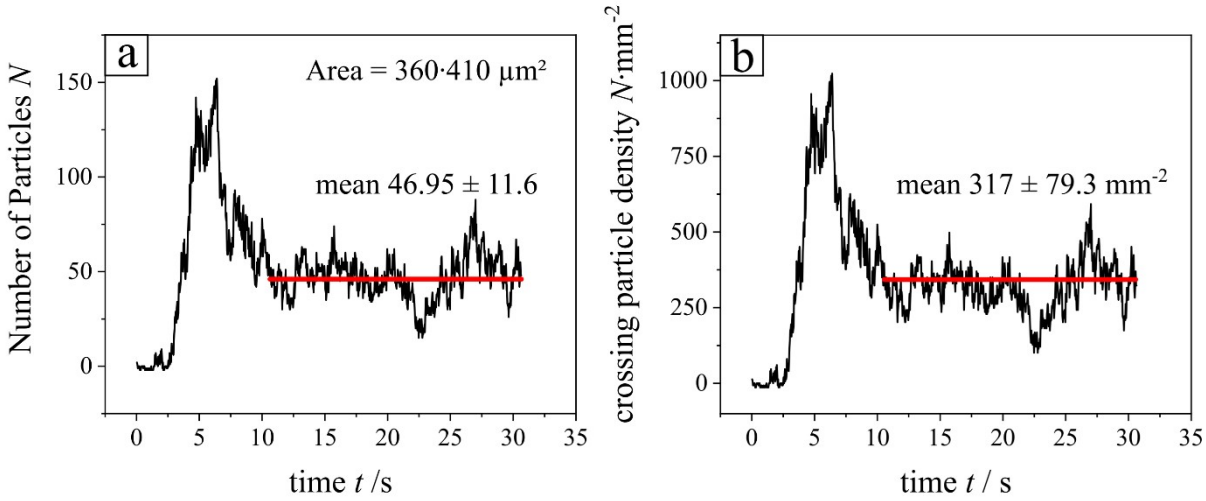

Figure S22. (a) number of porous particles crossing obstacle measured as function of the time. Detection area is 360·410 μm^2. (b) crossing particle density as a function of the time.

From **Video S6**, we quantified the number of porous colloidal particles traversing the top region of the channel by performing frame-resolved particles counting over a 30 s observation window immediately after illumination was switched on. The analyzed field of view was 360 · 410 μm², and the resulting time-dependent particle counts are presented in **Figure S22a**.

To enable comparison with the overall crossed particles, the measured counts were normalized by the average areal number density of crossing particles, also shown in **Figure S22b**. After illumination, porous particles exhibits a transient enhancement of crossing particles, which rapidly decays into a quasi-steady transport regime characterized by a constant number of

particles crossing the channel per unit time. The steady-state transport corresponds to a particle number flux of

$= 317 \pm 79.3\ s^{-1} \cdot mm^{-2}$,

which represents the areal throughput of separated particles across the channel cross-section.

To estimate the macroscopic separation throughput, we upscale this flux by multiplying it with the channel cross-sectional area (5 mm²) and the operation time (1 h), assuming a spatially homogeneous particle flux across the entire channel cross-section. Under this assumption, the total number of separated particles *N* can be expressed as

$$N_{sep} = \Phi \cdot t \cdot A = (79.25 \pm 20) \frac{1}{mm^2 \cdot s} \cdot 3600\ s \cdot 5\ mm^2 \quad \text{S28}$$

$$N_{sep} = 5.71 \cdot 10^6\ particles$$

where $A = 5\ mm^2$ and $t = 3600$ s.

Sample batchwise operation

From the reference system employing a microfluidic channel of comparable dimensions, approximately 7,500 particles were detected within an observation area of 3.3 × 3.3 mm² (10.89 mm²). In that study, the suspension contained a porous-to-plain particle ratio of 2:1, corresponding to a porous particle mass fraction of 0.66. For a total particle concentration of ctotal = 0.5 mg/mL the absolute concentration of porous particles is therefore

$c_{porous} = 0.66 \cdot c_{total} = 0.66 \cdot 0.5\ mg/mL = 0.33\ mg/mL$.

To extrapolate the particle inventory to the full microfluidic separation channel, we scale the counted particles to the effective channel footprint defined by the channel width $w = 5$ mm and length $L = 17$ mm, corresponding to an active area of 85 mm². Assuming a homogeneous particle distribution across the channel area, a simple proportional scaling yields.

$$N_{channel} = 7500 \cdot \frac{85}{10.89} \approx 58\,540 \text{ particles} \quad \text{S29}$$

for a single channel. According to the reference[1] operation parameters, approximately 20 min are required for the phototactic separation step. Including additional time for sample preparation, injection, and gravitational sedimentation (~10 min), the total process time per cycle amounts to 30 min. Consequently, two separation cycles can be performed per hour,

resulting in $N_{\text{hour}} = 58\,540 \cdot 2.$ To enable comparison with the continuous-flow separation experiment, the particle throughput is normalized to the porous particle concentration used in the present work, $c_{\text{porous}} = 0.1\ \text{mg mL}^{-1}$. Relative to the reference concentration $0.33\ \text{mg mL}^{-1}$, this corresponds to a scaling factor of $f = \frac{0.1}{0.33} \approx 0.3.$ Applying this concentration normalization yields an effective number of separated porous particles per hour of

$$N_{\text{sep}} = 58\,540 \cdot 2 \cdot 0.3 \approx 35\,478 \text{ particles.} \quad \text{S30}$$

Thus, under equivalent geometric and operational assumptions, the estimated hourly throughput corresponds to approximately 3.5×10^4 separated porous microparticles per channel.

Mass of one particle

$$V = \frac{4}{3} \cdot \pi \cdot a^3 = \frac{4}{3} \cdot \pi \cdot (2.5\ \mu m)^3 = 65.4\ \mu m^3 \quad \text{S31}$$

$$V = 6.54 \cdot 10^{-11} cm^3$$

With density of 1.8 g/cm³

$$m_P = \rho \cdot V = 1.8 \cdot 6.54 \cdot 10^{-11} cm^3 = 1.18\ 10^{-10} g \quad \text{S32}$$

and multiplying with N_{sep} this yields the total sample mass.

Sample mass for one hour

$$N_{sample\ per\ hour} = N_{sep} \cdot m_P \quad \text{S33}$$

$$N_{continous} = 5.71 \cdot 10^6 \cdot 1.18\ 10^{-10} g$$

$$N_{continous} = 6.72 \cdot 10^{-4} g = 0.672\ mg$$

$$N_{batch} = 35\,478 \cdot 1.18\ 10^{-10} g$$

$$N_{batch} = 4.18 \cdot 10^{-6} g = 0.004\ mg$$

S10. Optical Setup

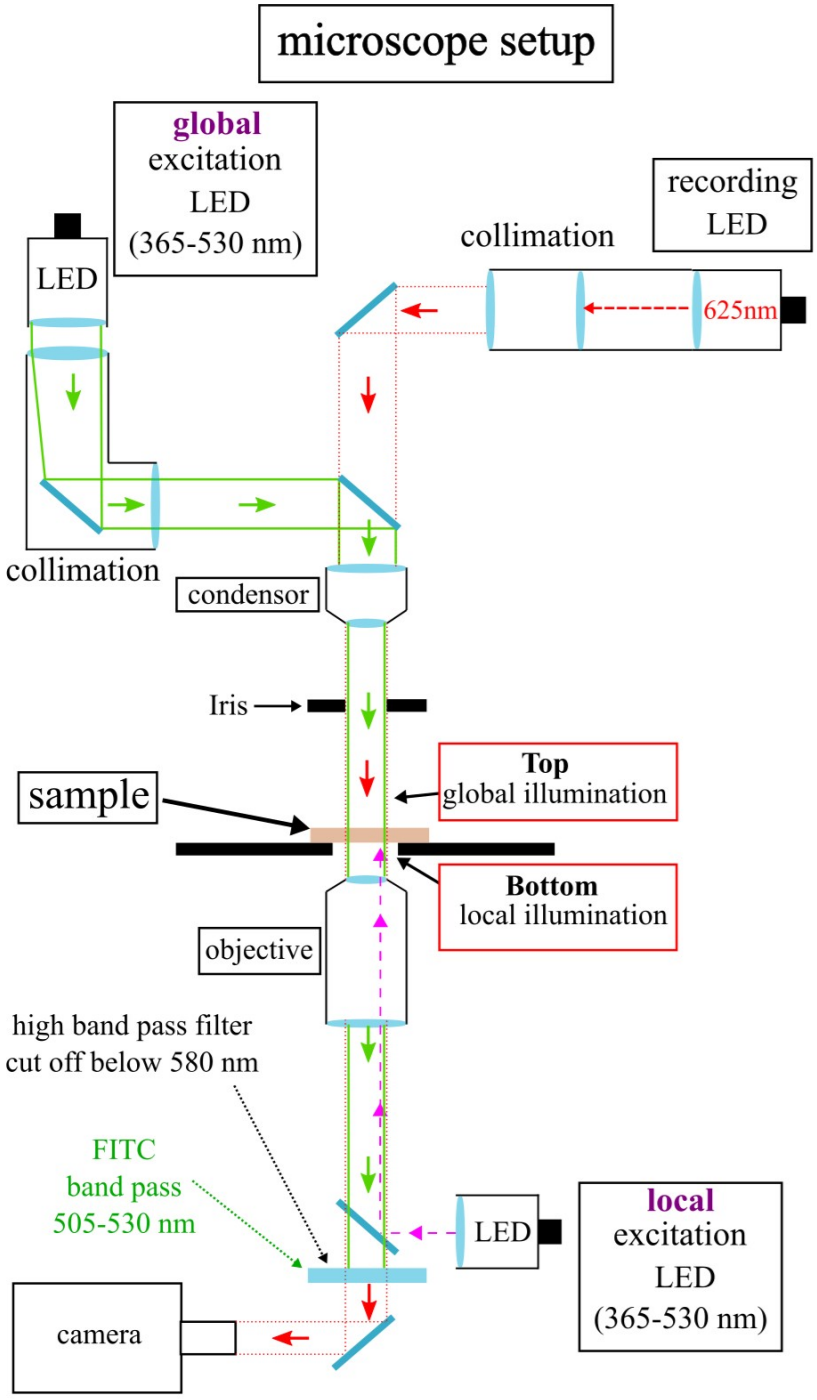

Figure S23. Schematic representation of optical microscope setup.

References for Supporting Information

[1] D. Vasquez Muñoz, F. Rohne, I. Meier, A. Sharma, N. Lomadze, S. Santer, M. Bekir, 2024, Light-Induced Material Motion Fingerprint – A Tool Toward Selective Interfacial Sensitive Fractioning of Microparticles via Microfluidic Methods, Small 20, 202403546. https://doi.org/10.1002/smll.202403546.

[2] M. N. Koleva, S. Liu, C. A. Styan, L. G. Papageorgiou, *Comput. Aided Chem. Eng.* **2016**, 38, 2379–2384.

[3] Lemmon, E. W.; Bell I. H.; Huber M. L.; and. McLinden M. O. Thermophysical Properties of Fluid Systems, NIST Chemistry WebBook, NIST Standard Reference Database Number 69, Eds. Linstrom P.J. and Mallard W.G., National Institute of Standards and Technology, Gaithersburg MD, 20899, https://doi.org/10.18434/T4D303, (retrieved January 12, 2026).

[4] Lemmon, E. W.; Bell I. H.; Huber M. L.; and. McLinden M. O. Isothermal Properties for Water, NIST Chemistry WebBook, NIST Standard Reference Database Number 69, Eds. Linstrom P.J. and Mallard W.G., National Institute of Standards and Technology, Gaithersburg MD, 20899, https://doi.org/10.18434/T4D303, (retrieved January 12, 2026).

[5] Tiesinga E.; Mohr P. J.; Newell D. B.; and Taylor B. N. Values of Fundamental Physical Constants, NIST Standard Reference Database 121, (retrieved January 12, 2026).

[6] Bekir, M., Sperling, M., Muñoz, D.V., Braksch, C., Böker, A., Lomadze, N., Popescu, M.N. and Santer, S. (2023), Versatile Microfluidics Separation of Colloids by Combining External Flow with Light-Induced Chemical Activity. Adv. Mater., 35: 2300358. https://doi.org/10.1002/adma.202300358

[7] M. Bekir, M. Sperling, D. V. Muñoz, C. Braksch, A. Böker, N. Lomadze, M. N. Popescu and S. Santer, *Adv. Mater.*, 2023, 35, 2300358. https://doi.org/10.1002/adma.202300358